coatings

Article

Correlation between the Rheological Properties of Asphalt Mortar and the High-Temperature Performance of Asphalt Mixture

Song Li [1,3], Xingxing Shi [2], Chundi Si [1,3], Binshuo Bao [4,*] and Mengmeng Hu [1]

1 School of Traffic and Transportation, Shijiazhuang Tiedao University, Shijiazhuang 050043, China; lisong@stdu.edu.cn (S.L.); sichundi@stdu.edu.cn (C.S.); humeng819@163.com (M.H.)
2 School of Civil Engineering, Shijiazhuang Tiedao University, Shijiazhuang 050043, China; a13015389791@126.com
3 State Key Laboratory of Mechanical Behaviour and System Safety of Traffic Engineering Structures, Shijiazhuang 050043, China
4 School of Management, Shijiazhuang Tiedao University, Shijiazhuang 050043, China
* Correspondence: baobinshuo@stdu.edu.cn

Abstract: The performance of an asphalt mixture is significantly affected by the properties of its asphalt mortar, which consists of an asphalt binder, mineral fillers, fine aggregates and air voids. The aim of this work was to evaluate the correlations between the high-temperature performance of an asphalt mixture and the rheological properties of its corresponding asphalt mortar. The multisequence repeated loading (MSRL) test was used to estimate the high-temperature performance of the asphalt mixture. Six different gradations, AC-13, SMA-13, SUP-13, AC-20, SUP-20 and AC-25, and two styrene–butadiene–styrene (SBS)-modified asphalt binders were considered and used to prepare the asphalt mixture specimens. The gradations and asphalt types of asphalt mortars were consistent with their asphalt mixtures. A modified multiple-stress creep–recovery (MSCR) test was proposed for evaluating the rheological properties of asphalt mortar with a dynamic shear rheometer (DSR). Based on the basic form of the Hirsh model, a multiple regression model was established, and its coefficient of determination (R-square) was 0.96. The rheological response of the asphalt mortar presented great correlation with the high-temperature behaviour of the asphalt mixture. In addition, the MSCR indicators (nonrecoverable compliance and percent recovery) obtained at 12.8 kPa creep stress represented the rheological status of asphalt mortar in asphalt mixture well. Therefore, the mechanical behaviours of asphalt mixture at high temperature could be accurately predicted by the MSCR indicators of asphalt mortar and its coarse aggregate parameters.

Keywords: asphalt mortar; high-temperature performance; rheological properties; multisequence repeated loading (MSRL) test; multiple-stress creep–recovery (MSCR) test

Citation: Li, S.; Shi, X.; Si, C.; Bao, B.; Hu, M. Correlation between the Rheological Properties of Asphalt Mortar and the High-Temperature Performance of Asphalt Mixture. *Coatings* **2023**, *13*, 1058. https://doi.org/10.3390/coatings13061058

Academic Editor: Valeria Vignali

Received: 15 May 2023
Revised: 3 June 2023
Accepted: 5 June 2023
Published: 7 June 2023

1. Introduction

Asphalt mortar can generally be regarded as a remaining part of removing coarse aggregate particles from an asphalt mixture structure. The asphalt mortar contains fine aggregates, mineral filler, asphalt binder and air voids, among others. It also can be referred to as a fine asphalt mixture (FAM) [1]. The asphalt mortar as a filling material between coarse aggregate gaps in asphalt mixture shows a significant relationship with the deformation, fatigue, cracking and healing properties of the asphalt mixture. However, there are no unified methods for the design and fabrication of asphalt mortar. Moreover, the key design indicators of asphalt mortar, including nominal maximum aggregate size (NMAS), asphalt binder content and air void content, greatly affect the performance of asphalt mortar.

For the NMAS of asphalt mortar, it is believed that the aggregate particle size in asphalt mortar does not exceed 1.18 mm [2]. Three asphalt mortars with an NMAS of 4.0 mm, 2.0 mm and 1.18 mm, respectively, have been studied, and the fatigue performance results of asphalt mortars with an NMAS of 2.0 mm are most similar to those of asphalt mixtures [3]. To date, there are no unified regulations of the NMAS limits in asphalt mortar. Therefore, the NMAS of asphalt mortar needs to be determined based on the model computation precision and image processing accuracy. It also should consider the specific testing conditions of target asphalt mortar specimens.

The content of asphalt binder in asphalt mortar should be consistent with the amount of asphalt mortar distributed among coarse aggregates in an asphalt mixture to ensure that research on the rheological performance of asphalt mortar and its correlation with asphalt mixture have practical significance. To ensure the real state of the asphalt mortar in its asphalt mixture, the asphalt binder content can be determined by the test methods of asphalt extraction and asphalt ignition combustion for the produced asphalt mixture specimen [4,5]. However, these methods consider the fine aggregate in the asphalt mixture and do not consider the asphalt mortar coated on the surface of the coarse aggregate. The asphalt binder content of asphalt mortar can be determined by the theory of asphalt film thickness in asphalt mixtures. Based on an assumption [2], 8.0% of the asphalt binder content in asphalt mortar can guarantee an asphalt film coating on a fine aggregate surface with an average thickness of approximately 10 μm. Karki [6] has also used an asphalt film thickness of 12 μm to determine the asphalt binder content in the asphalt mortar, and it is consistent with the true condition of the mortar portion of the asphalt mixture. In addition, the asphalt binder content in asphalt mortar can be better determined by the specific surface areas of aggregate particles. This method is simple and widely used [7]. To overcome the large deviation in the specific surface area method in modified asphalt mortar, Ng et al. [8] have considered the different asphalt binder absorptivity properties of fine aggregates to improve the calculation of asphalt binder content in asphalt mortar. The asphalt binder content for the asphalt mortars with different asphalt binder properties and fine aggregate types can be well determined.

The mechanical behaviour of an asphalt mortar is significantly affected by its air void content. As air voids in asphalt mixtures are distributed between asphalt mortars and coarse aggregates, some researchers have considered all air voids to be in the asphalt mortars [9]. Then, the amount of air voids in asphalt mortar is consistent with that in its asphalt mixture. The air void content in asphalt mortar can be determined according to the compaction density of the asphalt mixture. The mass and volume of asphalt mortar are determined by removing the coarse aggregate and its absorbed asphalt binder, and then the actual density of asphalt mortar is obtained [10]. Researchers have analysed the linear shear moduli of asphalt mortars with different air void contents and found that the shear moduli of asphalt mortars increase with decreasing air void content. If the air void content decreases by 1%, the shear moduli of asphalt mortars increase by approximately 7% [11].

The NMAS, asphalt binder content and air void content are the most important control indicators in the design and preparation of asphalt mortar. However, from recent research, there are no clear or unified methods for determining these control indicators. According to different theoretical assumptions and calculation models, the calculated control indicators are different. Therefore, the preparation of asphalt mortar should simulate its status in an asphalt mixture to the greatest extent to accurately analyse and explore the asphalt mixture's mechanical performance through asphalt mortar test results.

When the asphalt mixture shows inelastic or nonlinear behaviours, the asphalt mortar might exhibit microcracking or deformation, which is closely related to the overall mechanical performance of asphalt mixture [9]. Compared with asphalt binder, the scale of asphalt mortar is closer to that of the asphalt mixture [12]. Moreover, asphalt mortar is relatively close to the location where most fatigue and damage occur in asphalt mixture [2]. Therefore, as an intermediate material in asphalt mixture structure, the behaviour of asphalt mortar presents great correlation with its asphalt binder and asphalt mixture.

The evaluation methods and indicators of asphalt mortar can be determined for reference to the related laboratory tests of asphalt binders and asphalt mixtures. The complex shear modulus G^* can be used as an evaluation index of the high-temperature viscoelastic properties of asphalt mortar. Similar to the asphalt binder and asphalt mixture, the complex shear modulus G^* is the ratio of stress and strain applied to asphalt mortar under dynamic load conditions. According to the size of asphalt mortar, the G^* index value of asphalt mortar can be accurately obtained through a frequency scanning test conducted by dynamic shear rheometer (DSR) [13]. In the literature, a 0.01% strain is recommended as the linear viscoelastic boundary limit of asphalt mortar. It is believed that when the strain of asphalt mortar is less than 0.01%, asphalt mortar exhibits linear viscoelastic behaviour during loading [14,15]. Generally, asphalt mortar can be used as a model input to effectively predict the related properties of asphalt mixtures [16], which significantly reduces the test time and material cost.

To date, the relevant research on the high-temperature properties investigation are mainly focused on the asphalt binder and the asphalt mixture; the evaluation of the high-temperature response is mainly investigated through laboratory tests under dynamic loading modes to analyse the creep–recovery properties of the asphalt binder and the asphalt mixture [17,18]. The Federal Highway Administration (FHWA) has formed a multiple-stress creep–recovery (MSCR) test to evaluate the high-temperature performance of asphalt binders by adding stress cycles based on a repeated creep and recovery (RCR) test [19]. The MSCR test is commonly used in high-temperature viscoelastic performance tests and research evaluations for asphalt binder [20,21]. It has become one of the most promising methods for evaluating the high-temperature behaviour of asphalt binders. Recent studies have used the MSCR test to test the performance of modified asphalt binders [22,23]. It has been found that the MSCR test has the advantage of reflecting the elastic and viscoelastic properties for evaluating the rutting potential of modified asphalt binder. The cumulative strain of a composite modified asphalt is significantly reduced during the MSCR test. The composite modified asphalt is epoxy resin (ER) and crumb rubber powder (CRP) mixed into styrene–butadiene–styrene (SBS)-modified asphalt binder [24]. In addition, based on the MSCR test results, the urea formaldehyde–epoxy resin (UFE) microcapsule incorporation can improve the viscoelasticity, high-temperature stability and permanent deformation resistance of SBS-modified asphalt binder [25]. The MSCR test makes the asphalt binder fully exhibit creep–recovery mechanical properties in a high-temperature condition through repeated loading–unloading, which can verify its viscoelastic response well [7,26].

For the asphalt mortar, there are few standard laboratory experiments on the high-temperature performance of the intermediate-scale materials (i.e., asphalt mortar) and its relationship to asphalt mixtures. Because of the high contents of asphalt binder in the asphalt mortar and the feasibility of asphalt mortar samples for DSR equipment, the performance of asphalt mortar can be investigated for reference to the test methods of asphalt binder (i.e., MSCR test). The test procedures should be modified further in order to satisfy the characteristics of the asphalt mortar. The asphalt mixture behaviour can be well predicted by the properties of all its components, including asphalt binder, mineral filler, fine aggregate, coarse aggregate, etc. and their interactions. When the measured properties of asphalt mortar were adopted, the performance of asphalt mixture can be predicted regardless of the interactions of fine aggregate, mineral filler and asphalt binder in the asphalt mortar. In addition, the prediction model can be simplified significantly.

Therefore, in this paper, the high-temperature rheological properties of asphalt mortar were investigated by a modified MSCR test. In addition, a multisequence repeated loading (MSRL) test was used to investigate the high-temperature performance of the asphalt mixture. A prediction model for the high-temperature performance of asphalt mixtures based on the rheological response of asphalt mortar and properties of coarse aggregates was established. The correlation between asphalt mortar and its asphalt mixture was well investigated. The results of this study provide a new perspective for predicting the performance of asphalt mixtures. The research flowchart of this study is presented in Figure 1.

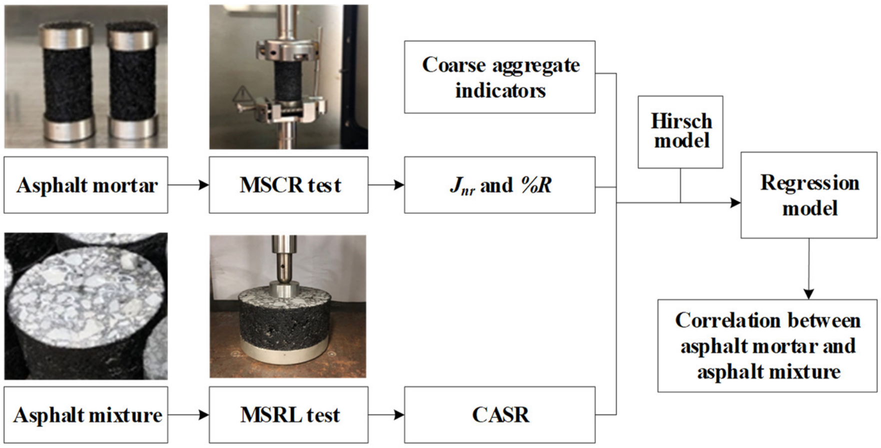

Figure 1. Research flowchart.

2. Materials and Methods

2.1. Materials Preparation

2.1.1. Asphalt Binder

In this paper, two kinds of styrene–butadiene–styrene (SBS)-modified asphalt binders were selected to prepare the asphalt mixture and asphalt mortar with SBS modifier contents of 3.0% and 3.5% of the asphalt binder mass, respectively. The high-temperature performance grading (PG) results of the modified asphalt binder with 3.0% and 3.5% SBS content were PG70 and PG76, respectively. Therefore, the above two modified asphalt binders in this paper were expressed by PG70 and PG76. The basic technical indicators of these two asphalt binders are shown in Table 1.

Table 1. Performance levels of asphalt binders.

Indicators	PG70	PG76
SBS content (ratio of binder by mass)	3.0%	3.5%
Softening point (°C)	65	76
Ductility (cm, 5 cm/min, 5 °C)	50	43
Penetration (0.1 mm, 100 g, 25 °C, 5 s)	52	54
$G^*/\sin\delta$ @70 °C for original binder (kPa)	1.93	2.15
$G^*/\sin\delta$ @76 °C for original binder (kPa)	1.15	1.44
$G^*/\sin\delta$ @70 °C for RTFOT binder (kPa)	2.88	3.56
$G^*/\sin\delta$ @76 °C for RTFOT binder (kPa)	1.60	2.87

Note: RTFOT—rolling thin film oven test. The RTFOT binder means the asphalt binder sample after the RTFOT and represents short-term-aged asphalt binder.

2.1.2. Aggregates and Fillers

In this paper, basalt and limestone aggregate particles commonly used in pavement construction were used to prepare asphalt mixture and asphalt mortar specimens. The asphalt mixture with an NMAS of 13.2 mm was composed of basalt aggregate, and the asphalt mixtures with NMASs of 19 mm and 26.5 mm were composed of limestone aggregate. The asphalt mortar corresponding to the asphalt mixture was prepared by the same type of fine aggregate particles. In this paper, 2.36 mm was selected as the particle boundary of coarse and fine aggregates; that is, fine aggregate particles forming asphalt mortar could pass through the 2.36 mm sieve. Mineral filler is limestone with a particle size of less than 0.075 mm.

2.1.3. Asphalt Mixture

The commonly used gradations of asphalt mixture in pavement structure were selected to fabricate the asphalt mixture specimens. These gradations of asphalt mixtures were used for high-temperature performance investigation of six gradation types of asphalt mixture, including AC-13, SMA-13 and SUP-13 in the upper layer, AC-20 and SUP-20 in the middle layer and AC-25 in the lower layer. Therefore, the design gradation results of these six asphalt mixtures are shown in Table 2.

Table 2. Gradation results of asphalt mixture.

	Gradations		Sieve Size (mm)											
			26.5	19	16	13.2	9.5	4.75	2.36	1.18	0.6	0.3	0.15	0.075
Passing percentage (%)	AC-13	UL	100	100	100	100	85	68	50	38	28	20	15	8
		LL	100	100	100	90	68	38	24	15	10	7	5	4
		DG	100	100	100	96.3	77.9	46.1	40.5	31.5	18.8	11.9	9.2	6.3
	SMA-13	UL	100	100	100	100	75	34	26	24	20	16	15	12
		LL	100	100	100	90	50	20	15	14	12	10	9	8
		DG	100	100	100	93.9	63.2	24.8	22.5	19.5	15.4	13.1	12.1	9.9
	SUP-13	UL	100	100	100	100	85	68	39.1	38	28	20	15	10
		LL	100	100	100	90	68	38	28	15	10	7	5	2
		DG	100	100	100	96.6	79.7	38.3	32.0	25.0	15.2	10.0	7.8	5.5
	AC-20	UL	100	100	92	82	72	56	44	33	24	17	13	7
		LL	100	90	74	62	50	26	16	12	8	5	4	3
		DG	100	100	87.3	80.9	60.9	40.1	31.0	23.4	14.3	10.3	8.2	6.8
	SUP-20	UL	100	100	92	82	72	56	34.6	33	24	17	13	8
		LL	100	90	74	62	50	26	23	12	8	5	4	2
		DG	100	100	82.5	73.9	54.5	36.4	28.2	21.3	13.2	9.6	7.7	6.4
	AC-25	UL	100	90	83	76	65	52	42	33	24	17	13	7
		LL	90	70	60	51	40	24	14	10	7	5	4	3
		DG	95.0	80.3	70.2	65.2	51.4	37.5	29.3	22.3	13.9	10.1	8.3	6.9

Note: UL—upper limit of gradation; LL—lower limit of gradation; DG—design gradation.

For the asphalt binder, PG70 and PG76 asphalt binders were used to prepare AC-13, SMA-13, SUP-13, AC-20 and SUP-20 asphalt mixtures, and PG70 asphalt binder was used to prepare AC-25 asphalt mixtures. The asphalt binder contents used in these six asphalt mixtures were 4.9%, 5.8%, 4.8%, 4.4%, 4.3% and 4.0%, respectively. In addition, lignin fibre was required to be added to the SMA-13 asphalt mixture, and the content was 0.3% of the mass of the SMA-13 asphalt mixture. The lignin fibre was bought from the manufacturer, and its length was less than 6.0 mm. All asphalt mixture specimens were formed using a gyratory compactor. The compacting times were limited by controlling the target height of the specimen to ensure that the number of compactions of each asphalt mixture was between 80 and 100, and the internal voidage of the specimen was controlled at approximately 4.0%. The asphalt mixture formed by gyratory compaction was a cylindrical specimen with a diameter of 150 mm and a height of 170 mm. The compacted specimens of asphalt mixture should be placed in a flat space for over 48 h at room temperature, and then the asphalt mixture specimen was obtained after the metal mould was removed.

To better explore the high-temperature properties of asphalt mixtures at different layers and meet the requirement of the MSRL test of asphalt mixture, the 150 mm diameter cylinder specimens of different types of asphalt mixture were cut into corresponding heights according to the layer height of pavement structure. The heights of specimens AC-13, SMA-13 and SUP-13, corresponding to the upper layer, were 40 mm; the heights of specimens AC-20 and SUP-20, corresponding to the middle layer, were 60 mm; and the height of specimen AC-25, corresponding to the lower layer, was 80 mm. Figure 2 shows the different types of final fabricated asphalt mixture specimens.

Figure 2. Asphalt mixture specimens.

2.1.4. Asphalt Mortar

Asphalt mortar is a mixture composed of fine aggregate particles, mineral filler, asphalt binder and voids. The rheological properties of asphalt mortar significantly influence the macro behaviour of asphalt mixtures. In this paper, all fine aggregate particles passing a 2.36 mm sieve were selected to prepare asphalt mortar samples. The fine aggregate gradation of asphalt mortar was obtained by equivalent calculation of the gradation curve of the asphalt mixture. In this paper, the asphalt mortar specimens corresponding to the six asphalt mixtures were represented by F-AC13, F-SMA13, F-SUP13, F-AC20, F-SUP20 and F-AC25, respectively. The equivalent fine aggregate gradation results are presented in Table 3. To better exhibit the gradations of different asphalt mortar samples, the grading curves of six asphalt mortars are shown in Figure 3.

Table 3. Gradation results of asphalt mortar.

Gradations		Sieve Size (mm)					
		2.36	**1.18**	**0.6**	**0.3**	**0.15**	**0.075**
Passing percentage (%)	F-AC13	100	76.9	44.3	26.8	19.7	12.3
	F-SMA13	100	82.9	59.0	46.2	40.2	27.5
	F-SUP13	100	77.5	46.3	29.5	22.7	15.3
	F-AC20	100	75.5	46.3	33.3	26.5	22.0
	F-SUP20	100	75.5	46.7	33.9	27.2	22.6
	F-AC25	100	76.0	47.3	34.6	28.3	23.5

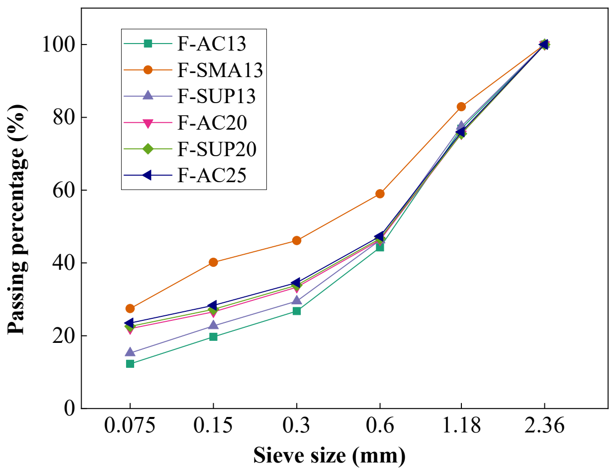

Figure 3. Gradation curve of fine aggregates of asphalt mortars.

The asphalt binder type in asphalt mortar samples was consistent with the asphalt mixture. F-AC13, F-SMA13, F-SUP13, F-AC20 and F-SUP20 were prepared with PG70 and PG76 asphalt binder, and F-AC25 asphalt mortar was prepared with PG70 asphalt binder. For the asphalt binder content of the asphalt mortar, the equivalent determination was made according to the asphalt binder content of the asphalt mixture, which is the equivalent amount of asphalt corresponding to fine aggregate and mineral filler particles in the asphalt mixture. In this paper, the specific surface area method of aggregate particles was used to equivalently calculate the asphalt binder content of asphalt mortar; that is, the thickness of the asphalt binder film coated on the aggregate surface was the same, the amount of asphalt binder was linearly correlated with the specific surface area of the aggregates and the equivalent asphalt binder content of asphalt mortar was calculated by the proportion of the specific surface area of the fine aggregate and mineral filler [27]. Therefore, based on the computing of specific surface area of aggregates [28], the calculation method of the equivalent asphalt binder content of asphalt mortar composed of fine aggregate particles of less than 2.36 mm is shown in Equations (1) and (2).

$$P_{a-mortar} = \frac{(SA_{<2.36}/SA) \times P_a}{P_{2.36}} \tag{1}$$

$$SA_{<2.36} = \sum (P_{<2.36} \times FA_{<2.36}) \tag{2}$$

where $P_{a\text{-}mortar}$ is the asphalt binder content of the asphalt mortar, and SA is the total specific surface area of all aggregate. $SA_{<2.36}$ is the total specific surface area of the aggregate passing through the 2.36 mm sieve, P_a is the optimal asphalt binder content of the asphalt mixture, $P_{2.36}$ is the passing percentage of the 2.36 mm sieve in the asphalt mixture, $P_{<2.36}$ is the passing percentage of aggregates smaller than 2.36 mm and $FA_{<2.36}$ is the surface area coefficient of aggregates smaller than 2.36 mm.

According to the calculations of Equations (1) and (2), the equivalent asphalt binder contents of the six asphalt mortars selected in this paper, F-AC13, F-SMA13, F-SUP13, F-AC20, F-SUP20 and F-AC25, are shown in Table 4.

Table 4. Asphalt binder contents of asphalt mortar samples.

	SA (m^2/kg)	$SA_{<2.36}$ (m^2/kg)	P_a (%)	$P_{2.36}$ (%)	$P_{a\text{-}mortar}$ (%)
F-AC13	5.906	4.975	4.9	40.469	10.2
F-SMA13	6.980	6.284	5.8	22.492	23.2
F-SUP13	5.051	4.221	4.8	32.048	12.5
F-AC20	5.497	4.669	4.4	30.974	12.1
F-SUP20	5.141	4.351	4.3	28.240	12.9
F-AC25	5.465	4.661	4.0	29.292	11.6

In this study, a DSR was used to investigate the high-temperature rheological properties of asphalt mortar. According to the size of the DSR loading fixture, the asphalt mortar samples were uniformly shaped into cylindrical specimens with diameters of 12 mm and heights of 30 mm. The asphalt mortar moulding mould was made of polytetrafluoroethylene material that did not stick to asphalt binder. The asphalt mortar mould is shown in Figure 4.

Asphalt mortar samples were prepared by manual mixing and compacting in the laboratory, and the mixing conditions of the asphalt mortar were consistent with the mixing process of the asphalt mixture. To ensure the homogeneity of the prepared asphalt mortar samples, after repeated trials and tests, the mixing and forming processes of asphalt mortar were summarized as follows.

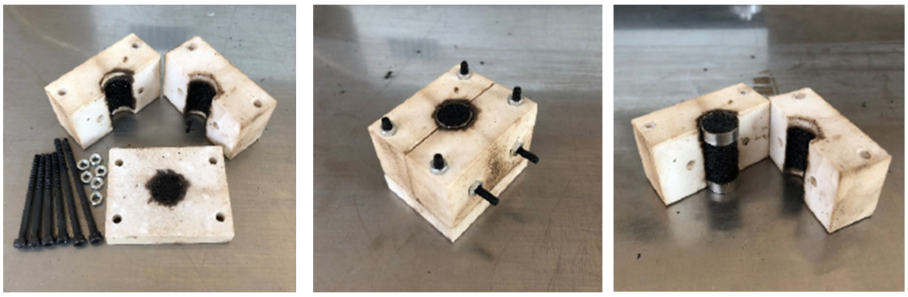

(a) (b) (c)

Figure 4. Mould of the asphalt mortar sample. (**a**) Mould composition, (**b**) mould structure and (**c**) sample in the mould.

Before mixing the asphalt mortar, each size of weighed fine aggregate and mineral filler was placed in an oven and stored at a constant temperature of 170 °C for 4 h. In addition, the metal cans and stirring rods used for mixing asphalt mortar were placed in the oven for heating. The SBS-modified asphalt binder (PG70 and PG76) was heated to 170 °C, and the quantitative asphalt binder was weighed according to the asphalt binder content of asphalt mortar. The asphalt binder was poured into the metal can with the fine aggregate, and the heated mixing rod was used to mix quickly and manually to ensure that the asphalt binder and fine aggregate were evenly coated in the shortest time. During the mixing process, the metal can was placed on the constant temperature heating furnace for heating to maintain the mixing temperature in the metal can between 165 °C and 170 °C. The mixing rod was manually used to continuously mix for at least 5 min. The mixed asphalt mortar bulk materials were weighed according to the mass required for each asphalt mortar sample. During compacting process, the asphalt mortar bulk material was added to the mould in four parts. After each addition of asphalt mortar, a heated stirring rod was used for manual compaction. The whole compaction process was fast and efficient to prevent the temperature of the asphalt mortar in the compacting process from decreasing too fast, which would affect the compaction effect. After all the weighed asphalt mortar bulk material was compacted into the mould, the top of the mould was covered with heavy objects and stored at room temperature. After 48 h, the mould was removed to obtain a complete asphalt mortar sample.

According to the above moulding method, the asphalt mortar samples with diameters of 12 mm and heights of 30 mm prepared are shown in Figure 5. In addition, each type of asphalt mortar could be moulded into four to five parallel asphalt mortar samples; three samples with better moulding effects were selected as the final samples of the asphalt mortar to undergo the rheological performance test.

Figure 5. Asphalt mortar moulding samples.

2.2. Laboratory Tests

2.2.1. Multisequence Repeated Loading Test of Asphalt Mixture

In this study, the MSRL test was used to evaluate creep behaviours of asphalt mixtures at high temperatures. The test conditions of asphalt mixture MSRL are usually consistent with the loading characteristics and temperature gradients of asphalt mixtures in actual pavement structures. The test results can reflect the high-temperature deformation abilities of asphalt mixtures in actual pavement structures well. According to the actual axle load of the pavement, the MSRL test applies six different stresses to the asphalt mixture specimen, and based on the stress condition of the actual pavement structure, stress ranges of 600 kPa to 1100 kPa, 500 kPa to 1000 kPa, and 300 kPa to 800 kPa are applied to the asphalt mixture specimens in the upper, middle and lower layers, respectively. In addition, according to the actual temperature gradient of the pavement structure, 62 °C, 58 °C and 52 °C were selected for the test temperatures of the asphalt mixture specimens in the upper, middle and lower layers, respectively. In the MSRL test, the loading frequency of all asphalt mixture specimens was the same as that of the standard dynamic creep test [29]: a single loading cycle of 1.0 s with a 0.1 s loading phase and a 0.9 s unloading phase. Each stress of the asphalt mixture specimen was loaded 100 times. At the beginning of the MSRL test, the preloading phase of 500 loading cycles is carried out. For the variability of the MSRL test, the loading sequence of each asphalt mixture specimen was repeated five times in the whole stress range, and the test results of the stress sequence in the stable stage are used to calculate the MSRL test index of the asphalt mixture. The strain rate (*SR*) and complex mean strain rate (*CASR*) are used to evaluate the creep properties of the asphalt mixture at high temperatures. The expressions of the evaluation indicators *SR* and *CASR* are shown in Equations (3) and (4). In addition, to take advantage of the confining pressure of the asphalt mixture specimens, all asphalt mixture specimens were subjected to the MSRL test with a 50 mm diameter indenter. The MSRL test conditions of the corresponding six asphalt mixtures in this paper are shown in Table 5.

$$\varepsilon = SR \times t + b \tag{3}$$

$$CASR = \frac{\sum_{i=1}^{n} SR_i}{n} \tag{4}$$

where ε is the asphalt mixture strain value for the MSRL test, *SR* is the strain rate corresponding to the stress of each loading order, t is the load action time under each stress condition (t = 1, 2, 3 . . . . . . , 100 s), b is the linear fitting constant, n is the number of stress levels in each loading sequence (n = 6) and *CASR* is the average composite strain rate of the asphalt mixture.

Table 5. Summary of MSRL test conditions for asphalt mixtures.

Asphalt Mixtures	**AC-13, SMA-13, SUP-13**	**AC-20, SUP-20**	**AC-25**
Asphalt binder	PG70, PG76	PG70, PG76	PG70
Test temperature	62 °C	58 °C	52 °C
Specimen size	Φ150 mm × 40 mm	Φ150 mm × 60 mm	Φ150 mm × 80 mm
Loading cycle	1.0 s (0.1 s + 0.9 s)	1.0 s (0.1 s + 0.9 s)	1.0 s (0.1 s + 0.9 s)
Loading stress	600, 700, 800, 900, 1000, 1100 kPa	500, 600, 700, 800, 900, 1000 kPa	300, 400, 500, 600, 700, 800 kPa
Preloading	700 kPa, 500 times	600 kPa, 500 times	400 kPa, 500 times
Loading times	100 times of each stress level	100 times of each stress level	100 times of each stress level

2.2.2. Multiple-Stress Creep–Recovery Test of Asphalt Mortar

The multiple-stress creep–recovery (MSCR) test is usually used to investigate the high-temperature rheological properties of asphalt binder in recent studies [26,30,31]. During the MSCR test, dynamic loading is applied to the asphalt binder specimens by DSR with controlled stress loading [32]. Based on the standard MSCR test for asphalt binder [33], the stresses of 0.1 kPa and 3.2 kPa are applied to the asphalt binder at 64 °C with DSR. Two evaluation indicators can be obtained. They are J_{nr} and $\%R$, named nonrecoverable compliance and percent recovery, respectively, which are used to evaluate the viscoelastic characteristics of asphalt binder at high temperature [34].

In this study, the MSCR test protocol was used to evaluate the high-temperature rheological properties of asphalt mortar. The asphalt mortar MSCR test was carried out at 64 °C with DSR test equipment. Due to the addition of fine aggregate particles in the asphalt mortar, it was necessary to install the loading fixture corresponding to the asphalt mortar specimen on the DSR to impose different grades of shear stress on the cylindrical asphalt mortar specimen with Φ12 mm × 30 mm and then complete the asphalt mortar MSCR test. The DSR insulation equipment and loading device for the asphalt mortar MSCR test are shown in Figure 6.

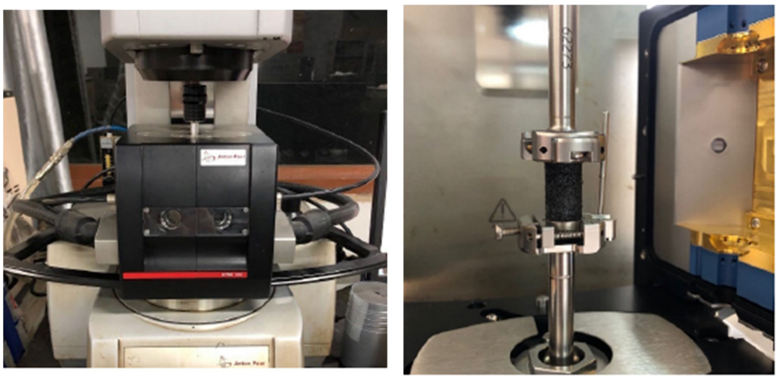

(**a**) (**b**)

Figure 6. Schematic diagram of asphalt mortar DSR equipment. (**a**) Asphalt mortar insulation device and (**b**) mortar sample loading fixture.

Based on the loading stress of the MSCR test of asphalt binder, combined with the sample size and stress conditions of asphalt mortar, the applied stress mode was modified in the asphalt mortar MSCR test. Then, the rheological properties of asphalt mortar were quantitatively evaluated by the MSCR test with eight stresses. The stresses applied in the test were 0.05 kPa, 0.1 kPa, 1.2 kPa, 2.4 kPa, 3.2 kPa, 6.4 kPa, 12.8 kPa and 25.6 kPa. The MSCR test of asphalt mortar adopted the loading mode of stress control, and each stress was loaded 10 times during the test. The single loading cycle included a 1.0 s loading stage and a 9.0 s unloading stage. The eight stresses were loaded step by step from low to high, and no time interval was set between different loading stresses. In addition, similar to the asphalt binder MSCR test, according to the creep–recovery strain curve of the asphalt mortar MSCR test, the two indicators of J_{nr} and $\%R$ were calculated to comprehensively evaluate the high-temperature rheological properties of asphalt mortar. The calculation expressions of J_{nr} and $\%R$ are shown in Equations (5)–(10).

$$\varepsilon_1 = \varepsilon_c - \varepsilon_0 \tag{5}$$

$$\varepsilon_{10} = \varepsilon_r - \varepsilon_0 \tag{6}$$

$$J_{nr}(N) = \frac{\varepsilon_{10}}{\sigma} \tag{7}$$

$$\%R(N) = \frac{(\varepsilon_1 - \varepsilon_{10})}{\varepsilon_1} \times 100\% = \frac{(\varepsilon_c - \varepsilon_r)}{\varepsilon_1} \times 100\% \tag{8}$$

$$J_{nr} = \frac{\sum_{N=1}^{10} J_{nr}(N)}{10} \tag{9}$$

$$\%R = \frac{\sum_{N=1}^{10} \%R(N)}{10} \tag{10}$$

where ε_0 is the initial strain at the beginning of the creep phase in each creep–recovery cycle, ε_c is the strain at the end of the creep phase in each creep–recovery cycle, ε_r is the strain at the end of the recovery phase in each creep–recovery cycle, σ is the stress applied in the MSCR test and N is the number of creep–recovery cycles under each stress (N = 1, 2, 3 . . . 10).

3. Results and Discussion

3.1. MSRL Test Results for Asphalt Mixture

In this study, the asphalt mixture specimens prepared by six different aggregate gradations and two SBS-modified asphalt binders were selected. According to the actual axial load conditions and temperature gradients of the upper, middle and lower layers, MSRL tests were carried out. The calculated results of the strain rate *SR* index values of different types of asphalt mixtures under different loading stress conditions are shown in Figure 7. In addition, according to the *SR* index results, the *CASR* index results of the complex average strain rate corresponding to all asphalt mixtures are shown in Figure 8.

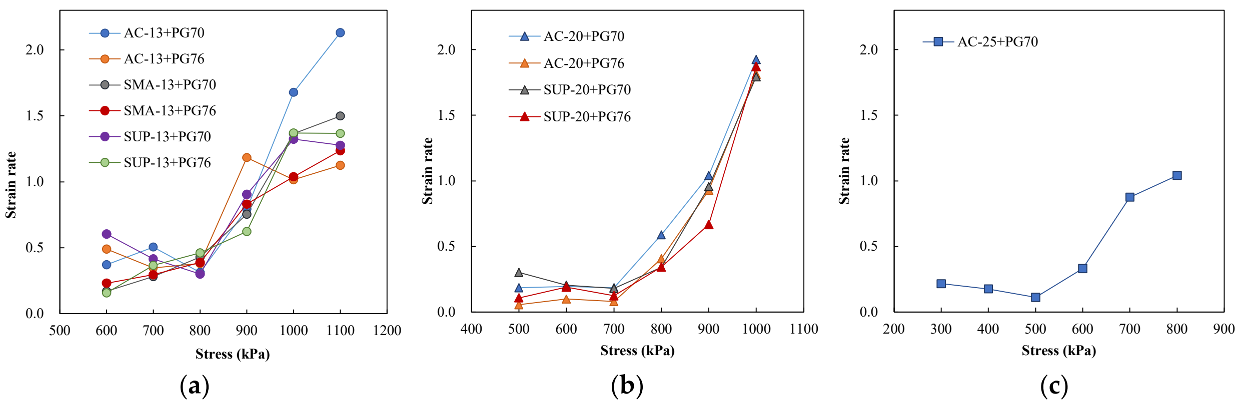

Figure 7. Results of the *SR* indicators of the asphalt mixture with different stresses. (**a**) Asphalt mixtures for the upper layer, (**b**) asphalt mixtures for the middle layer and (**c**) asphalt mixtures for the lower layer.

The *CASR* index of the asphalt mixture is the average result of the strain rate *SR* index under different stress conditions during the MSRL test, and it is a comprehensive evaluation index of the high-temperature performance of the asphalt mixture. Similarly, the smaller the *CASR* index value is, the higher the deformation resistance of the asphalt mixture and the better the high-temperature performance. As shown in Figure 8, the AC-25 asphalt mixture for the lower layer at 52 °C has the best resistance to deformation. Following are the AC-20 and SUP-20 asphalt mixtures for the middle layer at 56 °C. The high-temperature performance of the AC-13, SMA-13 and SUP-13 asphalt mixtures for the lower layer at 62 °C are the worst. The asphalt mixtures prepared with PG76 asphalt binder, with good viscoelastic properties at high temperature, are generally superior to that prepared with PG70 asphalt binder. In addition, among the asphalt mixtures with the same NMAS, SMA-13 has the strongest high-temperature deformation resistance, and the

SUP-13 and SUP-20 asphalt mixtures have slightly better high-temperature performance than the AC-13 and AC-20 asphalt mixtures, generally.

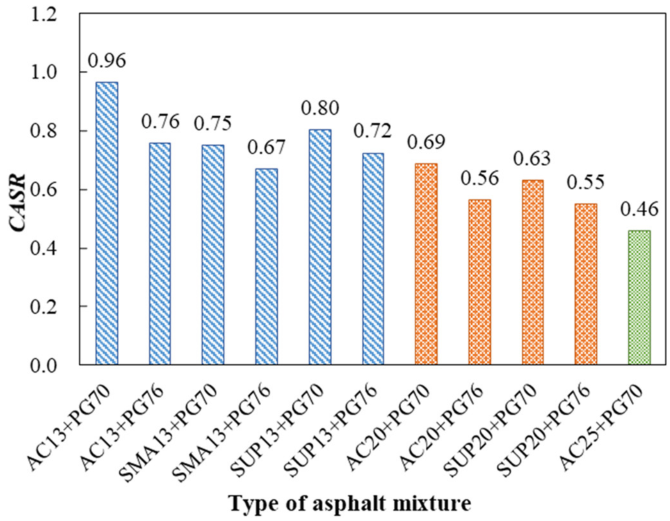

Figure 8. Asphalt mixture *CASR* index results.

3.2. MSCR Test Results of Asphalt Mortar

According to the calculation method of the evaluation indicators J_{nr} and $\%R$, the results of the J_{nr} and $\%R$ indicators of all asphalt mortars are shown in Figures 9 and 10. By analysing the MSCR test results of asphalt mortar, the J_{nr} and $\%R$ index values corresponding to small stresses of 0.05 kPa and 0.1 kPa are significantly different and do not conform to the loading response rules of different stresses of asphalt mortar. This finding may be because the modulus of asphalt mortar is large, the deformation resistance is strong and the small stress is insufficient for obvious torsional deformation. Then, in the creep–recovery process of the MSCR test, the testing instrument produces obvious data deviation with small loading stress. Combined with the variation laws of the J_{nr} and $\%R$ indicators of different asphalt mortars, the stress value of the asphalt mortar MSCR test should not be less than 1.2 kPa; thus, the asphalt mortar MSCR test results in this study are analysed within a stress range of 1.2 kPa–25.6 kPa.

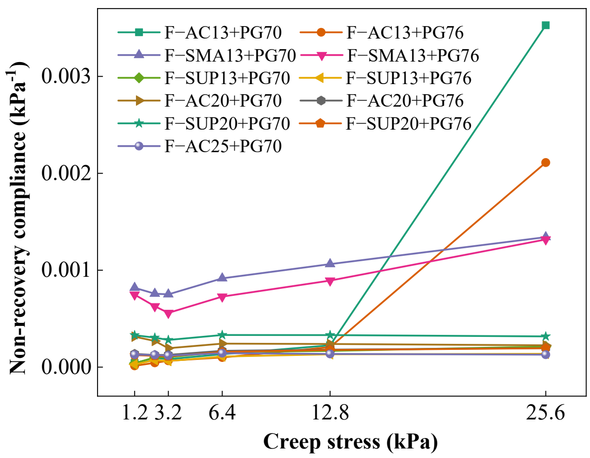

Figure 9. J_{nr} results of asphalt mortars.

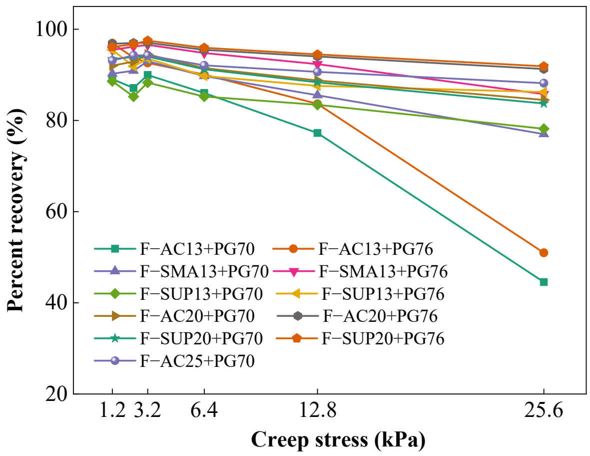

Figure 10. %R results of asphalt mortars.

In Figure 9, for the results of J_{nr} of asphalt mortar, the samples of F-SMA13+PG70 and F-SMA13+PG76 show relatively large values with various stresses. This phenomenon might be related to the gradation properties of the SMA-13 mixture and high asphalt binder content in the asphalt mortar of F-SMA-13. For the asphalt mortar of F-AC13, when the applied stresses are less than 12.8 kPa, their J_{nr} values are relatively small. When the applied stress increases to 25.6 kPa, the J_{nr} values of F-AC13 increase sharply. Generally, the sudden increase of J_{nr} for F-AC13 from 12.8 kPa to 25.6 kPa shows the asphalt mortar presenting significant nonlinear viscoelastic behaviour at 25.6 kPa. Obviously, F-AC13 asphalt mortar presented high stress sensitivity. Other gradations of asphalt mortars showed similar J_{nr} values and stress sensitivity.

For the %R results shown in Figure 10, F-AC20 and F-SUP20 asphalt mortars show relatively high %R values. This finding indicates that the asphalt mortars of F-AC20 and F-SUP20 present great elastic recovery performance. The asphalt mortar of F-AC13 shows reduced %R values and increased stress sensitivity, especially at large loading stresses. The asphalt mortar presents poor rheological properties.

Besides, for the different asphalt binder types, the J_{nr} index is lower and the %R index is higher for PG76 than for the PG70-modified asphalt binder under the same conditions. This result indicates that PG76 has better high-temperature performance and elastic recovery performance than PG70-modified asphalt binder.

3.3. Regression Model of Asphalt Mixture High-Temperatures Behaviour Based on Asphalt Mortar Properties

3.3.1. Parameter Determination of the Regression Model

The Hirsch model mainly considers the influences of the aggregate skeleton structures and asphalt binder viscoelastic characteristics on the high-temperature performance of asphalt mixtures [35,36]. Based on the above two influencing factors and their interactions, the high-temperature performance characteristics of asphalt mixtures can be better predicted. The specific expression of the Hirsch model is shown in Equations (11) and (12).

$$\begin{aligned}|E^*|_{mix} = P_c\left[4{,}200{,}000 \times \left(1-\frac{VMA}{100}\right)+3|G^*|_b\left(\frac{VFA\times VMA}{10{,}000}\right)\right]\\+(1-P_c)\left[\frac{1-(VMA/100)}{4{,}200{,}000}+\frac{VMA}{VFA\times 3|G^*|_b}\right]^{-1}\end{aligned} \quad (11)$$

$$P_c = \frac{\left(20+\frac{VFA\times 3|G^*|_b}{VMA}\right)^{0.58}}{650+\left(\frac{VFA\times 3|G^*|_b}{VMA}\right)^{0.58}} \quad (12)$$

where $|E^*|_{mix}$ is the dynamic modulus of the asphalt mixture, *VMA* is the voids in the mineral aggregate, *VFA* is the voids filled with asphalt binder, presenting effective asphalt binder saturation of asphalt mixture, and $|G^*|_b$ is the dynamic modulus of asphalt binder.

In the Hirsch model, the main factors affecting the high-temperature performance of asphalt mixtures include the voids in the mineral aggregate (*VMA*), effective asphalt binder saturation (*VFA*) and dynamic asphalt binder modulus G^*. According to the Hirsch model, asphalt mixtures can also be regarded as two-phase mixtures composed of asphalt mortar and coarse aggregate particles. When the input parameters are considered, the *VMA* can be replaced by the voids in the coarse aggregate (*VCA*) of coarse aggregate particles, and the effective asphalt saturation (*VFA*) can be replaced by the void filled with asphalt mortar (*VFF*), presenting asphalt mortar saturation, and the indicators of asphalt mortar are based on MSCR test results. The J_{nr} and $\%R$ indicators represent the viscoelastic properties of asphalt mortars at high temperatures. According to the above main influencing factors, a prediction model is established for the high-temperature performance of asphalt mixtures based on the rheological properties of asphalt mortars. Based on the calculation methods of the *VMA* and *VFA* indicators in asphalt mixtures [28], the calculation methods of *VCA* and *VFF* indicators in asphalt mixtures are determined. The expressions are shown in Equations (13)–(16). In this study, asphalt mortar is prepared from fine aggregates with particle sizes of less than 2.36 mm. Therefore, in the prediction model of the asphalt mixture, aggregate particles with sizes larger than 2.36 mm are all taken as coarse aggregate particles in the asphalt mixture, and the *VCA* index of coarse aggregate was calculated.

$$VCA = 100 - \frac{\gamma_f}{\gamma_{ca}} \times P_{ca} \tag{13}$$

$$P_{ca} = P_s \times PA_{2.36}/100 \tag{14}$$

$$\gamma_{ca} = \frac{P_{1c} + P_{2c} + \cdots + P_{nc}}{\frac{P_{1c}}{\gamma_{1c}} + \frac{P_{2c}}{\gamma_{2c}} + \cdots + \frac{P_{nc}}{\gamma_{nc}}} \tag{15}$$

$$VFF = \frac{VCA - VV}{VCA} \times 100 \tag{16}$$

where γ_f is the relative gross volume density of the asphalt mixture, γ_{ca} is the composite gross volume relative density of all coarse aggregates, P_{ca} is the percentage of all coarse aggregates in the total mass of the asphalt mixture, $PA_{2.36}$ is the 2.36 mm sieve residue in the aggregate gradation of the asphalt mixture, P_s is the sum of the percentage of all aggregates in the total mass of asphalt mixture, $P_{1c} \cdots P_{nc}$ is the percentage of various coarse aggregates in aggregate total mass, $\gamma_{1c} \cdots \gamma_{nc}$ is the relative density of gross volume of various coarse aggregates in aggregate and *VV* is the void fraction of asphalt mixture specimen.

3.3.2. *CASR* Regression Model of Asphalt Mixture

In this paper, the aggregate gradation and asphalt binder types commonly used in the upper, middle and lower layers of pavement structures were selected. A total of nine asphalt mixtures specimens, including AC-13+PG76, SMA-13+PG70, SMA-13+PG76, SUP-13+PG70, SUP-13+PG76, AC-20+PG70, AC-20+PG76, SUP-20+PG70 and AC-25+PG70, are used as the main research materials. In addition, the asphalt mortar samples corresponding to the above asphalt mixture are used to carry out asphalt mortar MSCR tests to obtain the high-temperature viscoelastic index of asphalt mortar. Notably, in the prediction model study, the MSCR test temperature of asphalt mortar is consistent with the MSRL test temperature of asphalt mixture. Therefore, MSCR tests at 62 °C, 58 °C and 52 °C are carried out for asphalt mortar samples. The sample information and test conditions of the asphalt mixture and asphalt mortar used to establish the prediction model are shown in Table 6.

Table 6. Summary of information of asphalt mixture specimens and asphalt mortar samples for establishing a regression model.

Pavement Layer	Upper Layer	Middle Layer	Lower Layer
Asphalt mixture	AC-13+PG76, SMA-13+PG70, SMA-13+PG76, SUP-13+PG70 and SUP-13+PG76	AC-20+PG70, AC-20+PG76 and SUP-20+PG70	AC-25+PG70
Asphalt mortar	F-AC13+PG70, F-SMA13+PG70, F-SMA13+PG76, F-SUP13+PG70 and F-SUP13+PG76	F-AC20+PG70, F-AC20+PG76 and F-SUP20+PG70	F-AC25+PG70
Asphalt mixture test	MSRL	MSRL	MSRL
Asphalt mortar test	MSCR	MSCR	MSCR
Test temperature	62 °C	58 °C	52 °C

According to the MSRL test results of the above nine asphalt mixtures and MSCR test results of asphalt mortar and the calculation results of the *VCA* and *VFF* indicators of the respective asphalt mixtures in Equations (13)–(16), the asphalt mixture *CASR* prediction model is established by the multivariate linear regression method. The fitting results of the *CASR* prediction models of the J_{nr} and $\%R$ index values under different stresses are shown in Figure 11.

According to the fitting results of the *CASR* prediction model for the asphalt mixture in Figure 11, the high-temperature performance of the asphalt mixture can be predicted well through the rheological indicators of asphalt mortar and the characteristic parameters of coarse aggregate; the prediction model obtained through multiple linear regression has a good goodness of fit. When the J_{nr} and $\%R$ indicators of asphalt mortar with different stresses are used for model fitting, the R^2 values are all greater than 0.89. The J_{nr} and $\%R$ indicators corresponding to 12.8 kPa of asphalt mortar have the best goodness of fit when fitting the *CASR* prediction model of the asphalt mixture, and the R^2 value is 0.96. Obviously, the high-temperature viscoelasticity of asphalt mortar under 12.8 kPa stress has the most significant correlation with the high-temperature performance of the asphalt mixture. Therefore, the fitting result corresponding to 12.8 kPa of asphalt mortar is used as the prediction model of the *CASR* index of the asphalt mixture, as shown in Figure 11e. The mathematical expression is shown in Equation (17).

$$
\begin{aligned}
CASR = &-21783.6282 \times J_{nr} + 1.1295 \times \%R - 0.2668 \times VCA + 2.3340 \times VFF \\
&+251.1547 \times (J_{nr} \times VFF) - 0.0127 \times (\%R \times VFF) - 197.4467
\end{aligned}
\tag{17}
$$

3.4. Validation of the CASR Regression Model for Asphalt Mixtures

In this paper, AC-13+PG70 and SUP-20+PG76 asphalt mixtures are used as model validation objects. By comparing the measured and predicted *CASR* index values of the asphalt mixture, the accuracy and reliability characteristics of the *CASR* prediction model of the asphalt mixture were verified. The J_{nr} and $\%R$ indicators and the calculation results of the *VFF* and *VCA* indicators under 12.8 kPa stress of asphalt mortar corresponding to the two asphalt mixtures are summarized in Table 7.

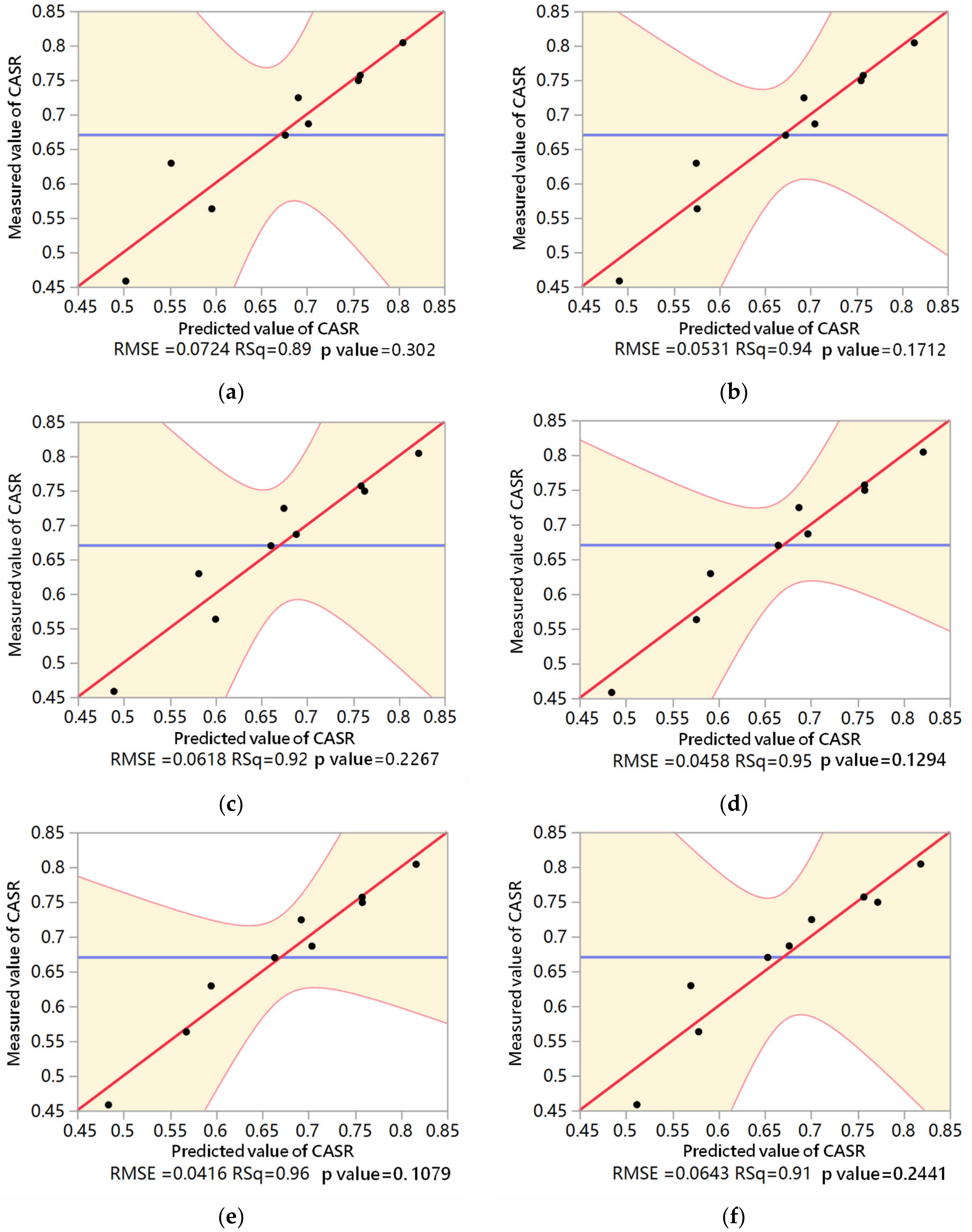

Figure 11. Results of fitting the *CASR* index of the asphalt mixture by the MSCR test index of asphalt mortar, *VCA* and *VFF* with different stresses. (**a**) 1.2 kPa, (**b**) 2.4 kPa, (**c**) 3.2 kPa, (**d**) 6.4 kPa, (**e**) 12.8 kPa and (**f**) 25.6 kPa.

Table 7. Comparison of measured and predicted results of the *CASR* index of the asphalt mixture.

Asphalt Mixture	J_{nr}-12.8	%*R*-12.8	*VCA*	*VFF*	Measured *CASR*	Predict *CASR*	Relative Error
AC-13+PG70	0.000225	77.257	49.447	91.911	0.965	1.041	7.86%
SUP-20+PG76	0.000180	94.031	40.133	90.033	0.563	0.568	0.91%

Therefore, the MSCR test results of asphalt mortar are strongly correlated with the high-temperature performance index of asphalt mixture *CASR*. Thus, the MSCR test results of asphalt mortar can characterize the high-temperature viscoelastic state of asphalt binder and predict the high-temperature performance of asphalt mixtures. The model can realize the effective connection between different scales of asphalt mixture materials.

4. Conclusions

In this paper, the correlation between the MSCR test of asphalt mortar and the MSRL test of asphalt mixture was established. The *VFF* values of asphalt mortar and the *VCA* values of coarse aggregate particles in asphalt mixture were proposed. Based on the Hirsh model, considering the results of the J_{nr} and %*R* indicators of asphalt mortar, *VFF* and *VCA* indicators, the *CASR* regression model of the asphalt mixture was established. The major conclusions were as follows:

1. The *SR* index of different asphalt mixtures was calculated through the MSRL test, and the composite average strain rate *CASR* index was obtained from the mean value of the *SR* index under different stresses. The test results of the high-temperature properties of the asphalt mixture measured by the MSRL test were in agreement with the general change law.
2. The MSCR tests of different kinds of asphalt mortars were carried out by DSR, and the nonrecoverable compliance J_{nr} and recovery percentage %*R* were used to quantitatively evaluate the viscoelastic properties of asphalt mortars at high temperatures. F-AC20+PG76 and F-SUP20+PG76 asphalt mortar samples had better elastic recovery performance. The asphalt mortar sample with PG76 asphalt binder had better high-temperature performance and elastic recovery performance than that with PG70 asphalt binder.
3. Based on the Hirsch model, the *CASR* regression model of asphalt mixtures was established by using the J_{nr} and %*R* index results of asphalt mortar and the *VFF* and *VCA* indicators results of asphalt mortar and coarse aggregate particles. Through verification, the model could accurately predict the high-temperature performance levels of asphalt mixtures.
4. Through regression model investigation, the index value of asphalt mortar under 12.8 kPa loading conditions in the MSCR test had the best correlation with the high-temperature properties of the asphalt mixture. Therefore, the MSCR test index of asphalt mortar under the stress condition of 12.8 kPa could best reflect its viscoelastic properties during asphalt mixture deformation at high temperatures.

It should be noted that the asphalt mixtures and asphalt mortars selected in this work were made of two types of asphalt binders and six types of aggregate gradations, which were commonly used in pavement engineering. The regression model was established by limited numbers of test data of asphalt mixture and asphalt mortar. Accurate explanation of properties of asphalt mortar and coarse aggregate and their interaction can improve accuracy of the prediction model, which would be considered in further studies.

Author Contributions: The authors confirm contribution to the paper as follows: analysis of results and draft manuscript preparation: S.L. and B.B.; laboratory test design and analysis: S.L., X.S. and M.H.; study conception and design: S.L. and C.S.; experimental work: S.L., X.S. and M.H. All authors have read and agreed to the published version of the manuscript.

Funding: This research was funded by Natural Science Foundation of Hebei Province, grant number E2022210054; Central Guidance on Local Science and Technology Development Fund of Hebei Province, grant number 226Z3801G; Introduction of Overseas-Educated Scholars Program of Hebei Province, grant number C20210306; Key R&D Project of Hebei Province, grant number 21373801D; Projects of Hebei Education Department, grant number SQ2021002 and SQ2022053.

Institutional Review Board Statement: Not applicable.

Informed Consent Statement: Not applicable.

Data Availability Statement: Data is contained within the article.

Conflicts of Interest: The authors declare no conflict of interest.

References

1. Suresha, S.N.; Ningappa, A. Recent Trends and Laboratory Performance Studies on FAM Mixtures: A State-of-the-Art Review. *Constr. Build. Mater.* **2018**, *174*, 496–506. [CrossRef]
2. Kim, Y.R. Mechanistic Fatigue Characterization and Damage Modeling of Asphalt Mixtures. Ph.D. Thesis, Texas A & M University, College Station, TX, USA, 2003.
3. Freire, R.A.; Babadopulos, L.F.A.L.; Castelo Branco, V.T.F.; Bhasin, A. Aggregate Maximum Nominal Sizes' Influence on Fatigue Damage Performance Using Different Scales. *J. Mater. Civ. Eng.* **2017**, *29*, 04017067. [CrossRef]
4. Sousa, P.; Kassem, E.; Masad, E.; Little, D. New Design Method of Fine Aggregates Mixtures and Automated Method for Analysis of Dynamic Mechanical Characterization Data. *Constr. Build. Mater.* **2013**, *41*, 216–223. [CrossRef]
5. Liu, X.; Liu, W.; Wang, S.; Wang, Z.; Shao, L. Performance Evaluation of Asphalt Mixture with Nanosized Volcanic Ash Filler. *J. Transp. Eng. Part B Pavements* **2018**, *144*, 04018028. [CrossRef]
6. Karki, P. Computational and Experimental Characterization of Bituminous Composites Based on Eexperimentally Determined Properties of Constituents. Master's Thesis, University of Nebraska Lincoln, Lincoln, NE, USA, 2010.
7. Wang, H.; Liu, X.; Apostolidis, P.; Wang, D.; Leng, Z.; Lu, G.; Erkens, S.; Skarpas, A. Investigating the High- and Low-Temperature Performance of Warm Crumb Rubber–Modified Bituminous Binders Using Rheological Tests. *J. Transp. Eng. Part B Pavements* **2021**, *147*, 04021067. [CrossRef]
8. Ng, A.K.Y.; Vale, A.C.D.; Gigante, A.C.; Faxina, A.L. Determination of the Binder Content of Fine Aggregate Matrices Prepared with Modified Binders. *J. Mater. Civ. Eng.* **2018**, *30*, 04018045. [CrossRef]
9. Im, S.; You, T.; Ban, H.; Kim, Y.-R. Multiscale Testing-Analysis of Asphaltic Materials Considering Viscoelastic and Viscoplastic Deformation. *Int. J. Pavement Eng.* **2017**, *18*, 783–797. [CrossRef]
10. Karki, P.; Kim, Y.-R.; Little, D.N. Dynamic Modulus Prediction of Asphalt Concrete Mixtures through Computational Micromechanics. *Transp. Res. Rec.* **2015**, *2507*, 1–9. [CrossRef]
11. Underwood, B.S.; Kim, Y.R. Experimental Investigation into the Multiscale Behaviour of Asphalt Concrete. *Int. J. Pavement Eng.* **2011**, *12*, 357–370. [CrossRef]
12. Li, S.; Ni, F.; Dong, Q.; Zhao, Z.; Ma, X. Effect of Filler in Asphalt Mastic on Rheological Behaviour and Susceptibility to Rutting. *Int. J. Pavement Eng.* **2021**, *22*, 87–96. [CrossRef]
13. Sadeq, M.; Al-Khalid, H.; Masad, E.; Sirin, O. Comparative Evaluation of Fatigue Resistance of Warm Fine Aggregate Asphalt Mixtures. *Constr. Build. Mater.* **2016**, *109*, 8–16. [CrossRef]
14. Kanaan, A.I.; Ozer, H.; Al-Qadi, I.L. Testing of Fine Asphalt Mixtures to Quantify Effectiveness of Asphalt Binder Replacement Using Recycled Shingles. *Transp. Res. Rec.* **2014**, *2445*, 103–112. [CrossRef]
15. Underwood, B.S. A Continuum Damage Model for Asphalt Cement and Asphalt Mastic Fatigue. *Int. J. Fatigue* **2016**, *82*, 387–401. [CrossRef]
16. Mignini, C.; Cardone, F.; Graziani, A. Correction to: Experimental Study of Bitumen Emulsion–Cement Mortars: Mechanical Behaviour and Relation to Mixtures. *Mater. Struct.* **2019**, *52*, 42. [CrossRef]
17. Zhang, L.; Xing, C.; Gao, F.; Li, T.; Tan, Y. Using DSR and MSCR Tests to Characterize High Temperature Performance of Different Rubber Modified Asphalt. *Constr. Build. Mater.* **2016**, *127*, 466–474. [CrossRef]
18. Mo, L.; Huurman, M.; Wu, S.; Molenaar, A.A.A. Mortar Fatigue Model for Meso-Mechanistic Mixture Design of Ravelling Resistant Porous Asphalt Concrete. *Mater. Struct.* **2014**, *47*, 947–961. [CrossRef]
19. D'Angelo, J.A. The Relationship of the MSCR Test to Rutting. *Road Mater. Pavement Des.* **2009**, *10*, 61–80. [CrossRef]
20. D'Angelo, S.; Ferrotti, G.; Cardone, F.; Canestrari, F. Asphalt Binder Modification with Plastomeric Compounds Containing Recycled Plastics and Graphene. *Materials* **2022**, *15*, 516. [CrossRef]
21. Turbay, E.; Martinez-Arguelles, G.; Navarro-Donado, T.; Sánchez-Cotte, E.; Polo-Mendoza, R.; Covilla-Valera, E. Rheological Behaviour of WMA-Modified Asphalt Binders with Crumb Rubber. *Polymers* **2022**, *14*, 4148. [CrossRef]
22. Li, M.; Luo, C.; Zhu, L.; Li, H.; Cong, P.; Feng, Y.; Yan, L. A Novel Epoxy-Terminated Polyethylene Modified Asphalt with Low-Viscosity and High Storage Stability. *Constr. Build. Mater.* **2022**, *335*, 127473. [CrossRef]
23. Pstrowska, K.; Gunka, V.; Prysiazhnyi, Y.; Demchuk, Y.; Hrynchuk, Y.; Sidun, I.; Kułażyński, M.; Bratychak, M. Obtaining of Formaldehyde Modified Tars and Road Materials on Their Basis. *Materials* **2022**, *15*, 5693. [CrossRef] [PubMed]

24. Lee, S.-Y.; Le, T.H.M. Laboratory and Full-Scale Testbed Study in the Feasibility of Styrene-Butadiene-Styrene Asphalt Pavement Having Epoxy Resin and Crumb Rubber Powder. *Buildings* **2023**, *13*, 652. [CrossRef]
25. Yang, S.; Ji, J.; Tao, H.; Muhammad, Y.; Huang, J.; Wang, S.; Wei, Y.; Li, J. Fabrication of Urea Formaldehyde–Epoxy Resin Microcapsules for the Preparation of High Self-healing Ability Containing SBS Modified Asphalt. *Polym. Compos.* **2021**, *42*, 4128–4137. [CrossRef]
26. Wasage, T.L.J.; Stastna, J.; Zanzotto, L. Rheological Analysis of Multi-Stress Creep Recovery (MSCR) Test. *Int. J. Pavement Eng.* **2011**, *12*, 561–568. [CrossRef]
27. Li, S. Multiscale Research on High-Temperature Creep Behaviour of Asphalt Mixture. Ph.D. Thesis, Southeast University, Nanjing, China, 2020. (In Chinese) [CrossRef]
28. *MOT, JTG E20-2011*; Standard Test Methods of Bitumen and Bituminous Mixtures for Highway Engineering. Ministry of Transport of the People's Republic of China: Beijing, China, 2011. (In Chinese)
29. Li, S.; Dong, Q.; Ni, F.; Jiang, J.; Han, Y. Evaluation of Susceptibility of High-Temperature Performance of Asphalt Mixture to Morphological Feature of Aggregates by Fractal Theory. *J. Mater. Civ. Eng.* **2018**, *30*, 06018018. [CrossRef]
30. Bastos, J.B.S.; Babadopulos, L.F.A.L.; Soares, J.B. Relationship between Multiple Stress Creep Recovery (MSCR) Binder Test Results and Asphalt Concrete Rutting Resistance in Brazilian Roadways. *Constr. Build. Mater.* **2017**, *145*, 20–27. [CrossRef]
31. Bao, B.; Liu, J.; Li, S.; Si, C.; Zhang, Q. Laboratory Evaluation of the Relationship of Asphalt Binder and Asphalt Mastic via a Modified MSCR Test. *Coatings* **2023**, *13*, 304. [CrossRef]
32. Delgadillo, R.; Bahia, H.U. The Relationship between Nonlinearity of Asphalt Binders and Asphalt Mixture Permanent Deformation. *Road Mater. Pavement Des.* **2010**, *11*, 653–680. [CrossRef]
33. *AASHTO, T350-14*; Standard Method of Test for Multiple Stress Creep Recovery (MSCR) Test of Asphalt Binder Using a Dynamic Shear Rheometer (DSR). AASHTO: Washington, DC, USA, 2018.
34. Ling, C.; Arshadi, A.; Bahia, H. Importance of Binder Modification Type and Aggregate Structure on Rutting Resistance of Asphalt Mixtures Using Image-Based Multi-Scale Modelling. *Road Mater. Pavement Des.* **2017**, *18*, 785–799. [CrossRef]
35. Alrashydah, E.I.; Abo-Qudais, S.A. Modeling of Creep Compliance Behavior in Asphalt Mixes Using Multiple Regression and Artificial Neural Networks. *Constr. Build. Mater.* **2018**, *159*, 635–641. [CrossRef]
36. Barugahare, J.; Amirkhanian, A.N.; Xiao, F.; Amirkhanian, S.N. ANN-Based Dynamic Modulus Models of Asphalt Mixtures with Similar Input Variables as Hirsch and Witczak Models. *Int. J. Pavement Eng.* **2022**, *23*, 1328–1338. [CrossRef]